nature structural & molecular biology

# On the structural basis of modal gating behavior in $K^+$ channels

Sudha Chakrapani[1–3], Julio F Cordero-Morales[1–3], Vishwanath Jogini[1,2], Albert C Pan[1,2], D Marien Cortes[1,2], Benoît Roux[1] & Eduardo Perozo[1]

**Modal-gating shifts represent an effective regulatory mechanism by which ion channels control the extent and time course of ionic fluxes. Under steady-state conditions, the $K^+$ channel KcsA shows three distinct gating modes, high-$P_o$, low-$P_o$ and a high-frequency flicker mode, each with about an order of magnitude difference in their mean open times. Here we show that in the absence of C-type inactivation, mutations at the pore-helix position Glu71 unmask a series of kinetically distinct modes of gating in a side chain–specific way. These gating modes mirror those seen in wild-type channels and suggest that specific interactions in the side chain network surrounding the selectivity filter, in concert with ion occupancy, alter the relative stability of pre-existing conformational states of the pore. The present results highlight the key role of the selectivity filter in regulating modal gating behavior in $K^+$ channels.**



Potassium channels are ubiquitous membrane proteins with a fundamental role in generation and modulation of the electrical excitability in cells[1]. Channel function is finely controlled by the interplay between activation gating at the stimulus-driven bundle crossing and C-type inactivation gating at the selectivity filter[2]. Recent high-resolution crystallographic analyses have provided atomic level details of $K^+$ channels trapped with the activation gate in the closed[3–5] or open conformation[6–9] and the inactivation gate in the conductive or nonconductive conformation[5,9].

A series of crystal structures of KcsA trapped in various degrees of gate opening and ion occupancy[9] have shown that entry into the C-type inactivated state is associated with a sequential reduction in ion occupancy at the S2 and S3 binding sites that is correlated to the extent of opening at the inner bundle gate. Although these structures provide unique insights into the basic structural transitions underlying the $K^+$ channel gating cycle, a cursory look at most single-channel recordings reveals that even the simplest ion channels show kinetically complex behaviors not fully explained by the present set of structures. This functional heterogeneity involves conductive and nonconductive states[10–13] as well as a variety of subconductance levels[12,14–17] for which there are no current structural correlates. We have provided evidence showing that under saturating stimulus conditions and at steady state (when the activation gate is in its fully open conformation), most of these gating fluctuations arise from conformational changes at the selectivity filter[11,12,18,19]. Not unexpectedly, the nature of the permeant ion[20–24] as well as a variety of mutations near the filter[17,25–28] have been shown to dramatically modulate the frequency and lifetimes of these gating events. In many cases, the structural consequences of these perturbations are reflected in changes in the ionic occupancy at the filter, which partly explains why these gating events diverge from normal functional behavior [26,29].

Modal gating appears to be a characteristic feature of many $K^+$ channels, in which time-dependent single-channel activity can switch abruptly between periods of high and low open probability, under fixed experimental conditions[30–32]. In several channels, differential inactivation rates underlie some of these gating regimes[31–34]. The KcsA selectivity filter and adjacent regions show considerable conformational flexibility, as revealed from a comparison of existing KcsA structures in high and low $K^+$ (ref. 5), in partial and fully open states[9], in the presence of blockers[35] and in the (so-called) 'flipped' structure observed in the E71A mutant[11]. It is easy to speculate that this intrinsic structural flexibility might underlie some of the heterogeneous functional behavior of the selectivity filter that leads to multiple gating modes[12].

Here we have investigated the functional and structural origins of modal gating in KcsA by studying a series of side chain substitutions at the Glu71 position. These mutations sharply reduce entry into the C-type inactivated state while stabilizing three kinetically defined gating modes, depending on the type of side chain at position 71. These gating modes are reminiscent of those seen in WT KcsA, based on their distinct intra-burst open probability ($P_o$), and were named high-$P_o$ mode (for mutants E71A, E71G, E71C, E71V, E71S or E71T), low-$P_o$ mode (E71I) and flickery mode (E71Q). High-resolution closed-state crystal structures of some of these mutations, together with molecular dynamics simulations, reveal changes in the ion profiles and water occupancy in and around the selectivity filter. These observations provide an initial rationale for explaining the origins of the conformational fluctuations that occur at the selectivity filter of the open-conductive channel.

[1]Department of Biochemistry and Molecular Biology, University of Chicago, Center for Integrative Science, Chicago, Illinois, USA. [2]Present addresses: Department of Physiology and Biophysics, Case Western Reserve University, Cleveland, Ohio, USA (S.C.); Department of Physiology, University of California San Francisco, San Francisco, California, USA (J.F.C.); D.E. Shaw Research, Hyderabad, India (V.J); D.E. Shaw Research, New York, New York, USA (A.C.P.); Department of Cell Physiology and Molecular Biophysics, Texas Tech University, Lubbock, Texas, USA (D.M.C.). [3]These authors contributed equally to this work. Correspondence should be addressed to E.P. (eperozo@uchicago.edu).

Received 20 March; accepted 18 October; published online 26 December 2010; doi:10.1038/nsmb.1968

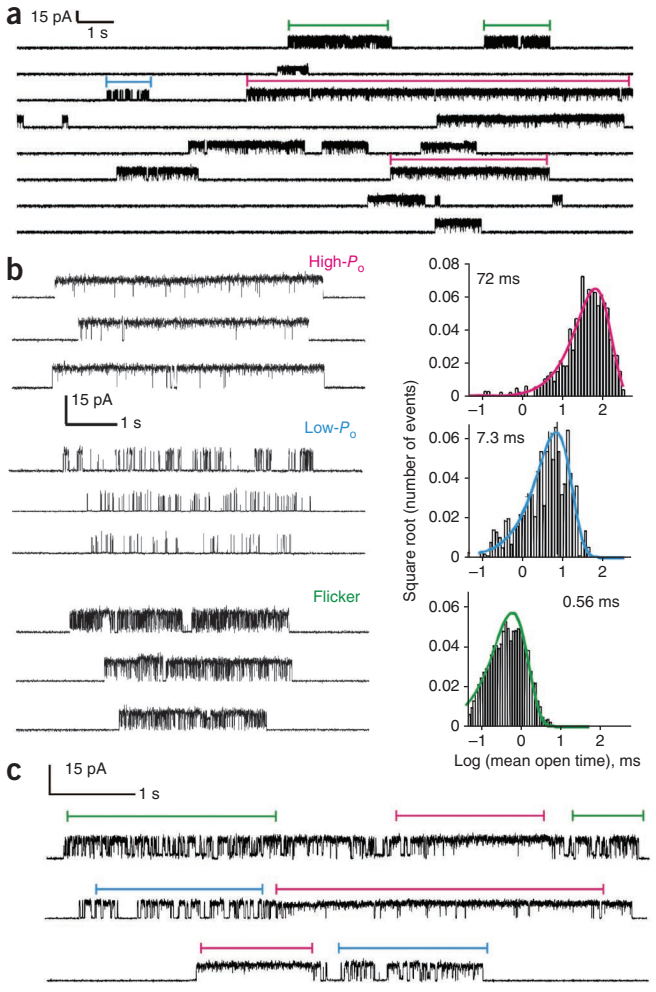


**Figure 1** Modal gating behavior of WT KcsA. (**a**) A continuous recording of KcsA single-channel currents measured under steady-state conditions at pH 3.0 and +150 mV in 200 mM symmetric $K^+$ solutions. (**b**) Left, KcsA shows a highly variable kinetic behavior that arises from a combination of three distinct modes of channel activity, the high-$P_o$, low-$P_o$ and flicker modes. Right, histograms show a distribution of open times within bursts for each of the three modes of channel activity with corresponding values indicated above. (**c**) Channels occasionally switch between modes within a burst of activity, suggesting that modes arise from a homogenous population of channels.

## RESULTS

### Variable modal kinetic behavior of wild-type KcsA

At steady state, and under saturating proton concentrations, KcsA predominantly resides in the nonconductive C-type inactivated state[11,12]. These long, silent periods are interrupted by brief sojourns into the conductive conformation followed by transitions back to the nonconductive inactivated state[11] (**Fig. 1a**). KcsA has been reported to show highly variable single-channel kinetic behavior, showing at least three distinct patterns or 'modes' of gating[12] (**Fig. 1b**). These modes are characterized by set variations in mean open and mean closed times: a high-$P_o$ mode with long open time $\tau_o \sim 100$ ms, a low-$P_o$ mode with intermediate open time $\tau_o \sim 10$ ms and a flickery mode with a very short open time $\tau_o < 1$ ms. The distribution of these modes is found to be random in nature, with no obvious evidence for pH or voltage dependence. The proportion of time spent in the individual modes varies greatly from one patch to another; however, the predominant mode is high-$P_o$. Steady-state, single-channel recordings show that transitions between modes can take place within the same burst (**Fig. 1c**), supporting the view that modal behavior in KcsA results from the conformational heterogeneity of individual channels. However, these transitions are infrequent, and modal changes are typically observed after sojourns in the C-type inactivated state.

### Mutations at position 71 stabilize diverse gating regimes

In voltage-dependent channels, modal gating has been associated with specific biochemical modifications[36,37], but the origin of KcsA's kinetic heterogeneity and subconductance levels has remained unclear. Mutations near the selectivity filter have been shown to substantially reduce this variability. In particular, the C-type inactivation–removing mutation E71A also unmasks kinetically homogeneous high-$P_o$ behavior, which is indistinguishable from the high-$P_o$ gating mode seen in wild-type (WT) KcsA[11,12]. We therefore carried out an in-depth analysis of the role of different side chain substitutions at position 71 on the steady-state single-channel kinetics of KcsA. Out of a total of 15 substitutions, 9 were well tolerated: alanine, cysteine, threonine, serine, valine, isoleucine, glutamine, histidine and glycine. Mutations to arginine, lysine, leucine, aspartic acid, asparagine and phenylalanine severely compromised channel folding and stability and were not analyzed further.

Analysis of macroscopic currents from the nine functional Glu71 mutants revealed that although there were no major effects on the time course of activation gating, the stability of the C-type inactivated state was directly affected by all mutations (**Fig. 2a**). As shown earlier[11,38], E71A eliminates C-type inactivation, E71H severely enhances it and E71S stabilizes an intermediate level. Mutants E71C, E71I, E71V, E71T and E71Q also slow down C-type inactivation with steady-state $P_o$ larger than 0.5 (**Fig. 2b**). The steady-state single-channel activity revealed by our analysis faithfully reflected the macroscopic behavior of each of the mutants, in which the long silent periods characteristic of WT KcsA recordings (>100 ms) were mostly absent (**Fig. 2c**).

However, the key observation from this set of mutants is that, besides slowing down C-type inactivation, these side chain substitutions displayed unique intraburst kinetic patterns arising from differences in the duration of opening and closing dwell times. Substitutions to alanine, glycine, cysteine, threonine, valine and serine resulted in a common phenotype with long opening bursts and few short intraburst closures. Substitution to isoleucine resulted in very homogenous kinetics with similar mean open and closed times, whereas substitution to glutamine led to sustained, high-frequency flickering behavior with very short open and closed sojourns. Notably, substitution to glycine also reduced the single-channel conductance by a factor of 10 (to 1.2 pA), a feature that was also reflected in the small amplitude of its macroscopic currents.

Overall, mutations that slowed down inactivation resulted in very homogenous kinetic behavior (**Supplementary Fig. 1**). All of the tested Glu71 mutants were fully selective to $K^+$ against $Na^+$ under bi-ionic conditions (**Fig. 2d**). Given the homogeneity of the kinetic behavior of these mutants and the obvious similarities between this behavior and that of the pre-existing gating modes in WT KcsA, we chose the mutants that best represented each type of kinetic mode for further analysis: E71A for the high-$P_o$ mode, E71I for the low-$P_o$ mode and E71Q for the flickery mode (highlighted by gray-shaded areas in **Fig. 2c**).

### Kinetic analysis of Glu71 mutants

The high open probability of E71A, E71I and E71Q (>0.7) allowed us to easily target recordings arising from a single active

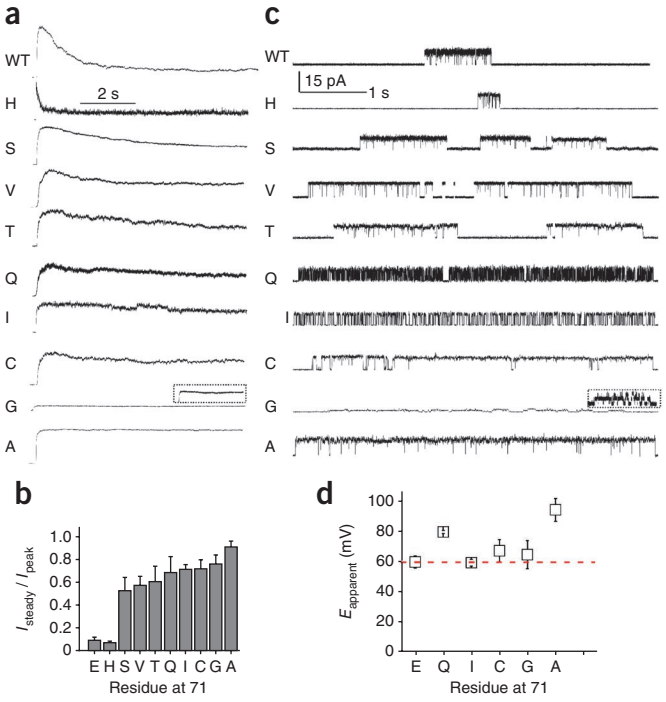


**Figure 2** Glu71 mutants stabilize individual gating modes in a side chain–specific way. (**a**) Macroscopic responses of WT and various Glu71 mutants elicited by pH jumps from 8.0 to 4.0 using a rapid solution exchanger in the presence of 200 mM KCl and with the membrane potential held at +150 mV. The current trace for the E71G mutant is shown at a relative amplitude compared with the other traces; the inset shows the same trace expanded in the current axis. (**b**) A plot of $I_{steady}/I_{peak}$ for various Glu71 mutants ($n > 5$). (**c**) Single-channel currents were recorded under steady-state conditions at pH 4.0 and +150 mV in 200 mM symmetric $K^+$ solutions. Gray box highlights mutants that are focused on in this study. (**d**) Selectivity versus $Na^+$ estimated from single-channel current-voltage (*I-V*) ramps under bi-ionic conditions. No detectable $Na^+$ currents were seen in any of the mutants. $E_{apparent}$ is the voltage value at which outward $K^+$ currents can last be resolved. Error bars, s.d ($n > 5$).

channel. Consequently, experiments carried out at different proton concentrations confirmed that the effect of increasing pH is mostly to decrease the burst length, as a result of the closure of the activation gate, with no major effects on the behavior of the burst itself. This is a clear indication that the transitions within the burst fully reflect the conformational fluctuations at the selectivity filter (**Supplementary Fig. 2**).

The rate constants to and from the conductive state for the various gating mode mutants were determined by fitting open and closed dwell-time distributions to a model with one conductive and three nonconductive states (**Fig. 3**). These three nonconductive states were defined as the "slow" inactive state ($I_s$), with dwell time ($\tau_c$) around 100 ms; an intermediate inactive state ($I_i$) with dwell time between 1 and10 ms; and the flicker (F) state, with dwell time in the 0.1–0.5-ms range. This classification is based on the lifetimes from single WT KcsA patches[11,12]. The behavior of the severely C-type inactivated mutant E71H was also analyzed to set a kinetic baseline for the transitions from a fully inactivated state. In **Figure 3** (right panels), the kinetic schemes and the shaded region show the predominant transition in each of the mutants. Our key observation is that each mutation is associated with changes in the rate constants governing transitions to and from each of the states that define modal gating in KcsA. Thus, whereas the E71Q mutation mostly affects transitions into and out of the F state, E71I favors transitions to $I_i$ and E71H is fundamentally biased toward $I_s$. As expected, most Glu71 mutants had a profound influence on the lifetime of $I_s$, which might suggest that destabilization of $I_s$ is a precondition to the stabilization of the $I_i$ or F state.

Individual rate constants derived from the fitted experimental dwell-time distributions of our basic four state model (**Table 1**), were used to simulate single-channel and macroscopic ensemble currents. Because these mutants did not alter activation, we used rate constants previously determined for WT KcsA to describe the proton-dependent transitions[12]. As expected, the models reproduced all of the unitary characteristics of the different gating modes as well as the time course for the macroscopic responses to pH pulses (**Supplementary Fig. 3**).

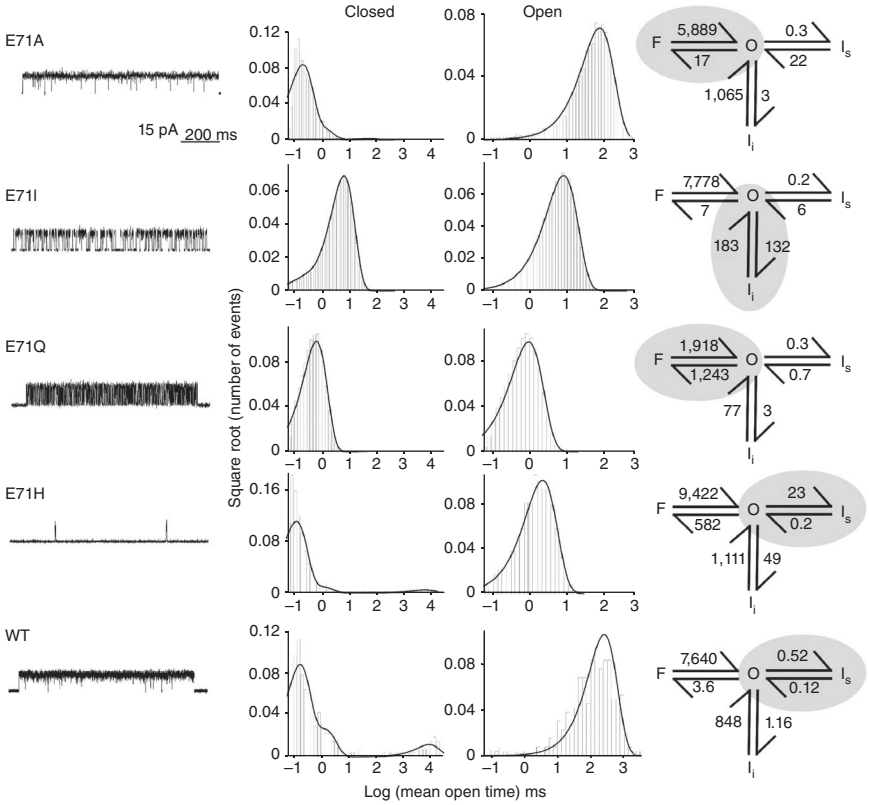


**Figure 3** Kinetic behavior of Glu71 mutants. Left, representative single-channel activity for Glu71 mutants. Middle, histograms show a distribution of closed- and open-channel lifetimes for the entire recordings. Single-channel current recordings were best fit by three closed and one open state for Glu71 mutants. Right, the closed states were defined as F, $I_i$ and $I_s$ on the basis of their lifetimes. Rate constants of recovery from $I_s$ for WT and E71H are overestimated as a result of low $P_o$ and uncertainty in the number of channels in the patch.

**Table 1 Kinetic parameters of the model**

| | F → O | F ← O | $I_i$ → O | $I_i$ ← O | Is → O | Is ← O | N |
|---|---|---|---|---|---|---|---|
| WT | 7,983 ± 1,739 | 5.6 ± 1.34 | 526 ± 30 | 0.9 ± 0.3 | 0.09 ± 0.01 | 0.45 ± 0.07 | 3 |
| E71A | 6,339 ± 268 | 10.9 ± 4.8 | 1,055 ± 291 | 2.2 ± 0.9 | 14.0 ± 3.4 | 0.22 ± 0.10 | 3 |
| E71I | 6,814 ± 287 | 21 ± 11.0 | 152 ± 59 | 151 ± 58 | 2.1 ± 1.9 | 0.33 ± 0.17 | 5 |
| E71Q | 1,972 ± 115 | 1,342 ± 187 | 97 ± 66 | 3.5 ± 1.6 | 1.86 ± 1.2 | 0.34 ± 0.34 | 5 |
| E71H | 7,906 ± 1,853 | 325 ± 128 | 526 ± 30 | 44.2 ± 11.8 | 0.18 ± 0.02 | 24.0 ± 1.0 | 3 |

### Crystal structures reveal subtle changes in ion occupancy

The discovery of individual mutants that greatly stabilized each of the major gating modes in KcsA provided a unique opportunity for us to investigate the structural basis of each gating mode. As the E71A structure is already available in the putative conductive conformation (closed inner gate)[11], we focused on mutations E71I and E71Q, which favor the $I_i$ and F states, respectively. Crystals of mutants E71I and E71Q were obtained as Fab complexes, diffracting at resolutions of 2.3 Å and 2.7 Å, respectively, and were solved by molecular replacement methods[5], using the structure of WT KcsA (1K4C) as a search model.

Experimental $2F_o - F_c$ electron density maps corresponding to the filter region and $F_o - F_c$ omit maps for the ion distribution profile are shown in **Figure 4** for E71I and **Figure 5** for E71Q. Overall, the selectivity filter structures of all gating mode mutants (**Figs. 4** and **5**) showed no major changes in backbone conformation and thus correspond to the filters observed in most closed KcsA structures, which adopt a conductive conformation (r.m.s. deviation with respect to 1K4C is 0.25 Å for E71I and 0.12 Å for E71Q). This result was not surprising, given that these mutations decrease the rate and extent of C-type inactivation and should indeed stabilize the conductive conformation. However, close observation of the electron density maps around the filter region revealed interesting differences between the mutants, in terms of the relative ion occupancy and the number of water molecules behind the filter (**Figs. 4** and **5**).

The one-dimensional electron density profile along the pore axis of E71I points to a clear loss of ion occupancy at the S2 binding site, together with an apparent decrease in the occupancy at S1 (**Fig. 4b**). On the other hand, the E71Q mutant shows a modest increase in the occupancy at the S2 binding site in comparison to WT KcsA (**Fig. 5b**). Beside these changes, the most striking difference among the mutants is the number of water molecules buried between the pore helix and the selectivity filter, bridging the filter region to the rest of the protein. In WT KcsA, a water molecule is coordinated by hydrogen bond interactions with Glu71, Asp80 and the backbone of Tyr78 in the selectivity filter. In the E71I structure, the 'cavity' formed by the reduced side chain volume is filled by three crystallographic water molecules interacting with the filter through a network of hydrogen bonds connecting the backbone of Gly79, Asp80, Leu81 and Tyr78 and the carboxyl group in Asp80 (**Fig. 4c**,**d**). There was no observable coordinated water in this region in E71Q (**Fig. 5c**,**d**), but this is likely due to resolution issues (at 2.7 Å).

### Glu71 mutants affect filter conformational dynamics

With the availability of individual crystal structures underlying each of the major gating modes, we then addressed the question of whether increased stability of the $I_i$ and F states in the E71I and E71Q mutants might be reflected in the conformational fluctuations of the filter. Molecular dynamics simulation studies suggest that water molecules behind the selectivity filter can affect the filter's conformational flexibility during ion permeation[39]. The timeframes of the single-channel transitions observed for $I_i$ and F (and of course, $I_s$) can be orders of magnitude away from the dynamic window available to straightforward molecular dynamics simulations; however, the present structures offer a unique opportunity to evaluate short-timeframe differences that might point to subsequent events directly linked to these gating transitions. We carried out a series of 20-ns simulations for mutants E71A, E71I, E71Q and E71G along with WT KcsA in a fully explicit system embedded in a lipid bilayer.

From these simulation runs, we observed two events of particular interest. The first observation is that the amide plane at Val76-Gly77 in the selectivity filter (in one of the subunits at a given time) underwent a 180° reorientation, pointing the backbone carbonyl oxygen of Val76 away from the conduction pathway (**Fig. 6a**). This type of transition has been observed in a number of molecular dynamics simulations[40–43] and leads to the loss of a favorable interaction at the S3 binding site, potentially affecting the associated free-energy barrier to translocation of $K^+$ from $S_3$ to $S_2$[44]. A plot of the backbone torsion angle as a function of the simulation time shows that the outward-facing (away from the conduction pathway) Val76 carbonyl is greatly stabilized in E71Q, where this conformation occurs at least ~40% of the total simulation time in a single subunit (**Fig. 6b**). In contrast, the Val76 carbonyl remained outward facing some 13% of the time

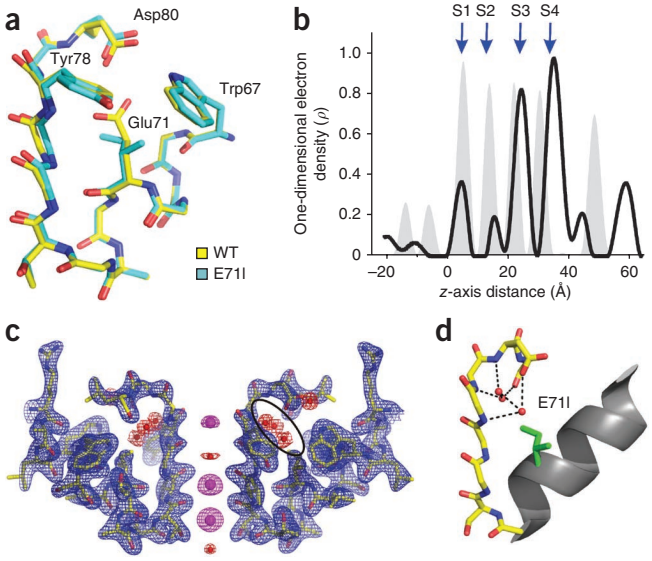


**Figure 4** Crystal structure of E71I. (**a**) Single-subunit line representation of the P-loop of E71I overlaid onto the WT structure[5] (PDB entry 1K4C) highlights the conductive conformation of the selectivity filter backbone. (**b**) One-dimensional electron density profile along the central symmetry (*z*) axis is shown. S1–S4 denote the $K^+$ binding sites. Gray peaks in the background correspond to one-dimensional electron density profile of the WT structure. (**c**) Electron density map of residues 60–84 from two diagonally symmetric subunits. Sticks, polypeptide chain; blue mesh, 2σ contour of the $2F_o - F_c$ electron density map for the protein; magenta mesh, 6σ contour of the $F_o - F_c$ omit map for the ions; red mesh, 4σ contour of the $F_o - F_c$ omit map for the waters. (**d**) A single-subunit P-loop is shown, with side chains at Glu71 and Asp80 in stick representation. The H-bond interaction between the three crystallographic water molecules within the cavity behind the filter and the rest of the protein are represented by black dotted lines.

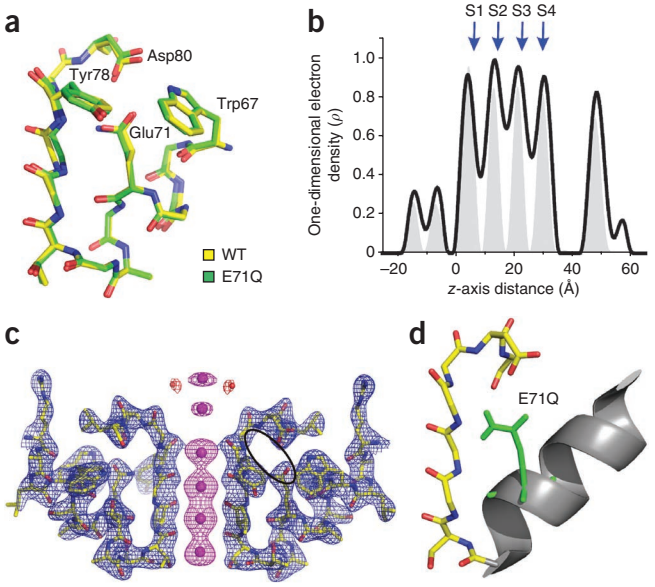


**Figure 5** Crystal structure of E71Q. (**a**) Single-subunit line representation of the P-loop of E71Q overlaid onto the WT structure[5] (PDB entry 1K4C) highlights the conductive conformation of the selectivity filter backbone. (**b**) One-dimensional electron density profile along the central symmetry (*z*) axis is shown. S1–S4 denote the $K^+$ binding sites. Gray peaks in the background correspond to one-dimensional electron density profile of the WT structure. (**c**) Electron density map of residues 60–84 from two diagonally symmetric subunits. Sticks, polypeptide chain; blue mesh, 2.5σ contour of the $2F_o - F_c$ electron density map for the protein; magenta mesh, (4–6)σ contour of the $F_o - F_c$ omit map for the ions; red mesh, 5σ contour of the $F_o - F_c$ omit map for the waters. (**d**) A single-subunit P-loop is shown, with side chains at Glu71 and Asp80 in stick representation. At 2.7-Å resolution, we observe no crystallographic waters within the cavity behind the filter.

in WT KcsA but only 3% of the time in the E71I mutant (**Fig. 6b**). At the functional level, the dwell-time ratio between the flicker and open states in the E71Q mutation was approximately 40:60 (**Fig. 3**), essentially mirroring the ratio of outward-facing to straight conformations in the simulation above.

Given the known differences in the timescales of single-channel kinetic and molecular dynamics simulations, this comparison between relative populations of states in simulations with the single-channel kinetics represents only part of a global sequence of events and at best should be considered only as a qualitative piece of the filter dynamics puzzle. Still, we note that out of five simulation runs (WT, E71A, E71I, E71Q and E71G), only the flicker-prone E71Q mutant showed a considerable increase in the frequency and lifetime of Val76 reorientation (**Fig. 6** and **Supplementary Fig. 4**). Therefore, we would like to suggest that the reorientation of the Val76 carbonyl might indeed be associated with the conformational changes that eventually lead to short-lived flicker states in single-channel records.

The second observation involves the outward 'flipping' of the Asp80 side chain relative to its position in WT KcsA, a movement reminiscent of the conformation observed in one of the crystal forms of E71A[11] (the so-called 'flipped' structure) and in the selectivity filter of Kir 3.1 (ref. 45). Monitoring the Cα-Cα distance between Glu71 and Asp80 reveals a very narrow distribution in WT KcsA, indicative of a strong interaction between these two residues (**Fig. 6c**, top). On the other hand, E71Q and E71I show a broader distribution, with a distinct second population that corresponds to channels with 'flipped' Asp80 (**Fig. 6c**, middle and bottom). In fact, this dual-population behavior is observed in all gating mode mutants at position 71, suggesting that the overall mobility of the Asp80 side chain is enhanced when there is no interaction with Glu71 (**Fig. 6** and **Supplementary Fig. 5**).

## DISCUSSION

$K^+$ channel stationary gating is known to involve nonconductive kinetic states with lifetimes ranging from submillisecond to several seconds. Transitions between these nonconductive states and conductive states define burst properties at the single-channel level, whereas changes in the equilibrium between these gating events lead to gating mode shifts. Modal gating is a common feature in a wide range of channels, particularly $K_v$[30–32], $Na_v$[34], $Ca_v$[46–48] and BK[49,50] channels as well as the AChR[51–53] and NMDA receptors[54,55]. In some channels, the mechanism for modal interconversion is subject to cellular control via phosphorylation and other post-translational modifications[30,31,36,37,56], but the molecular underpinning of these events has remained unknown in the majority of channels. In this study, we show that kinetically diverse conformational states that

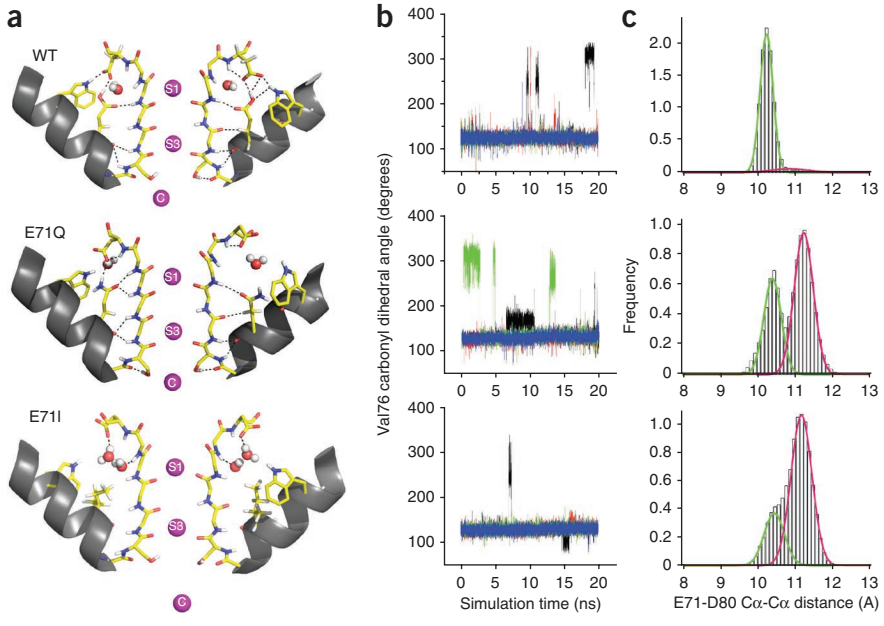


**Figure 6** Underlying conformational dynamics of the selectivity filter and the fast gating kinetics. (**a**) Structural snapshots of outward-facing carbonyl conformations. (**b**) Dynamics of carbonyl reorientation in KcsA. Time traces of the Val76 carbonyl dihedral angle (N-CA-C-O) during 20-ns molecular dynamics trajectories. Different colored lines correspond to different subunits. Potassium ions were initially placed in the cavity and sites S1 and S3. (**c**) Distribution of Glu71-Asp80 Cα-Cα distances. The green and magenta fits correspond to populations with Asp80 facing down (centered at ~ 10.3 Å) and 'flipped' outward (centered at ~ 11.1 Å), respectively.

**Table 2 Data collection and refinement statistics**

| | E71Q | E71I |
|---|---|---|
| **Data collection** | | |
| Space group | *I*4 | *I*4 |
| Cell dimensions | | |
| $a = b$, $c$ (Å) | 155.7, 76.1 | 156.4, 76.0 |
| $\alpha = \beta = \gamma$ (°) | 90 | 90 |
| Resolution (Å) | 40–2.7 | 40–2.3 |
| $R_{merge}$ (%) | 6.9 (36.3) | 8.0 (32.4) |
| $I/\sigma I$ | 17.5 (3.7) | 20.0 (2.7) |
| Completeness (%) | 94.0 (93.2) | 96.1 (94.3) |
| Redundancy | 6.1 (3.1) | 3.9 (3.1) |
| **Refinement** | | |
| Resolution (Å) | 40–2.7 | 40–2.3 |
| No. reflections | 23,689 | 39,318 |
| $R_{work}/R_{free}$ (%) | 22.6/26.8 | 26.4/27.1 |
| No. atoms | | |
| Protein | 4,074 | 4,073 |
| Ligand/ion | 7 | 5 |
| Water | 4 | 7 |
| *B*-factors | | |
| Protein | 59.2 | 45.7 |
| Ligand/ion | 41 | 51 |
| Water | 52 | 82.4 |
| R.m.s. deviations | | |
| Bond lengths (Å) | 0.007 | 0.005 |
| Bond angles (°) | 1.36 | 1.11 |

give rise to modal gating shifts can also originate from conformational fluctuations at or near the filter. Conveniently, each of the naturally occurring modes in KcsA can be individually stabilized, depending on the nature of the side chain at position 71 in the pore helix. Given that a wide range of mutations in our study converged on a limited set of gating modes, we suggest that the various side chain substitutions at position 71 do not introduce new kinetic behaviors but actually modulate the relative stability of pre-existing conformational states that are intrinsic to WT KcsA. These states were defined by their intrinsic dwell-time distributions (each roughly tenfold faster), as the slow (or deep) inactivated state $I_s$, the intermediate inactivated conformation $I_i$ and the highly fluctuating F or flicker state.

The question still remains as to why the WT channel shows gating heterogeneity, whereas mutants show more homogenous behavior. One common feature among these mutations is a substantial loss of C-type inactivation, and given that modes arise predominantly as channels recover from this inactivated state, it is likely that mode switches are associated with channel transitions between the deep inactivated and a series of open conductive conformations. These transitions might have slightly different energy paths, therefore causing heterogeneous behavior in WT KcsA.

The structural snapshots that underlie the molecular events leading to C-type inactivation ($I_s$) have recently been defined crystallographically[9]. These include a sequential loss of ion-binding sites S2 and S3, a pinching of the permeation pathway at Gly77 and a compression of the filter along the fourfold symmetry axis. The crystal structures and molecular dynamics simulations of the E71I and E71Q mutations offer insights into the short-lived $I_i$ and F states, respectively.

Ion occupancy in the E71I mutant filter is almost fully lost at S2 and partially decreased at S1, an ion profile that is distinctly different from that seen in either the fully conductive or the C-type inactivated filter[9]. We propose that this conformation of the filter is related to the intermediate $I_i$ state, for two reasons. First, even with the loss of external ion binding sites, the backbone conformation is essentially that of the fully conductive filter. In comparison, loss of S2 and a partial loss of S3 in an incompletely inactivated C-type filter leads to obvious changes in the filter backbone[9]. Second, recovery from C-type inactivation has been shown to be sensitive to external permeant ion concentration and to the ability of the ion to move from one site to another[57]. Given the easy access of S1 to the external bulk $K^+$, ion rebinding at S1 is expected to be more favorable than at S2 and S3. We therefore suggest that during permeation in WT KcsA, loss of ions at the external binding sites leads to the intermediate $I_i$ states, whereas sequential vacancies at the deeper S2 and S3 sites lead to the more stable, fully developed C-type inactivated ($I_s$) state.

Another interesting feature of this structure relates to the variation in the number and location of water molecules coordinated in the cavity behind the selectivity filter. In WT KcsA, a water molecule links the carboxyl groups on Glu71 and Asp80 with the backbone amides of Tyr78 and Gly79 in the conductive conformation, but two water molecules coordinate these residues in the collapsed, low $K^+$ structure[5]. Substitution of Glu71 with isoleucine results in three water molecules that generate extensive H-bonding interactions with the backbones of residues Gly79, Leu81 and Tyr78, and the Asp80 side chain. Although the precise effect of substituting the functionally important E71-D80 interaction for the three waters of coordination is as yet unknown, it is tempting to speculate that the resulting H-bond network would promote the stabilization of $I_i$ and the relative destabilization of the conductive conformation of the filter, the O state.

Our molecular dynamics simulations suggest that the frequency of spontaneous reorientation transitions of the Val76 carbonyl group is greatly enhanced in the E71Q mutation but is mostly unaffected in the rest of the mutants. However, given the wide differences in timescale between our experimental and computational data, it is difficult to establish a direct correlation between the dwell time of the outward-facing carbonyl conformation (nanosecond timescale) and the kinetics of single-channel flicker events (microsecond timescale). Clearly, it is unlikely that one carbonyl Val76 reorientation corresponds to one flicker event observed in electrophysiology. Identifying a mutant that displays an increase in the frequency of flickers with parallel increases in the incidence of Val76 reorientation allows us to suggest that these transient carbonyl-reorientation events, which accompany ion translocation from one binding site to the next during permeation, may also trigger transitions that lead to short-lived flicker states. The reorientation of Val76 might be an 'initiating' event that leads to subsequent nonconductive conformations of the selectivity filter. These conformations would be metastable in the microsecond timescales, as has been suggested on the basis of equivalent molecular dynamics runs[44].

Simulation runs further revealed a bimodal distribution of Asp80 side chain positions for all of the Glu71 mutations (except E71H). The existence of these two conformations is not surprising if we consider that the loss of the interaction with Glu71 should enhance the mobility of Asp80. It is interesting to note that the enhanced flexibility of Asp80 is also reflected in an increase in the crystallographic B-factor of this region in the E71I crystal structure (**Supplementary Fig. 6**). We believe that the additional conformational freedom of Asp80 leads to a decrease in the backbone constraints at Tyr78 and Gly79, with obvious consequences to the overall conformational dynamics of the filter. However, it still remains unclear how this motional freedom relates to the different gating forms seen in WT KcsA. Because most voltage-dependent $K^+$ channels have a valine at the position corresponding to Glu71 in KcsA, some of these conformational fluctuations of the filter might play a role in other members of the $K^+$ channel family.

In conclusion, the pore helix, selectivity filter and external vestibule are dynamic structures where small, local conformational changes (which include motions of the carbonyl oxygens, small fluctuations of the filter backbone, or changes in the configuration and occupancy of water molecules behind the filter) can have drastic effects on gating. These structural changes modulate the interplay between ions and the filter and thus underlie the diverse gating patterns observed in single-channel recordings of most $K^+$ channels. In KcsA, selectivity filter fluctuations are defined by a complex energy landscape that includes three kinetically distinct gating fluctuations. Transitions into each of the different gating modes depend on the relative depth of the energy wells associated with the three pre-existing selectivity filter conformations.

## METHODS

Methods and any associated references are available in the online version of the paper at http://www.nature.com/nsmb/.

**Accession codes.** The atomic coordinates of the mutants E71I and E71Q have been deposited in the Protein Data Bank under accession codes 3OR7 and 3OR6, respectively.

*Note: Supplementary information is available on the Nature Structural & Molecular Biology website.*


### ACKNOWLEDGMENTS

We thank F. Bezanilla, L. Cuello, V. Vásquez and H. Raghuraman for insightful discussions; M. Wiener and M. Purdy for crystallographic data collection (for E71Q); the staff of the SER-CAT 22-ID and GM/CA-CAT 23-ID beamlines at the Advanced Photon Source, Argonne National Laboratory, for their invaluable assistance in data collection; R. MacKinnon (Rockefeller University) for providing the KcsA antibody hybridoma cell line; and the US National Center for Supercomputing Applications (NCSA) and the Laboratory Computing Resource Center (LCRC) at Argonne National Laboratory for computer time. This work was supported by US National Institutes of Health grants to E.P. (R01GM057846, U54GM087519) and B.R. (R01GM062342) and by an American Heart Association Postdoctoral Fellowship to S.C.


### AUTHOR CONTRIBUTIONS

S.C., J.F.C.-M. and E.P. designed the research. S.C. and J.F.C.-M. carried out electrophysiology measurements and kinetic analysis. D.M.C. made Fab preparations. J.F.C.-M. and D.M.C. crystallized the mutant proteins. V.J. determined and analyzed the structures. A.C.P. and B.R. did the computation analysis. S.C., J.F.C.-M. and E.P. analyzed the data and wrote the paper.

### COMPETING FINANCIAL INTERESTS

The authors declare no competing financial interests.

Published online at http://www.nature.com/nsmb/.
Reprints and permissions information is available online at http://npg.nature.com/reprintsandpermissions/.


1. Hille, B. *Ion Channels of Excitable Membranes* (Sinauer Associates Inc., 2001).
2. Yellen, G. The moving parts of voltage-gated ion channels. *Q. Rev. Biophys.* **31**, 239–295 (1998).
3. Doyle, D.A. *et al.* The structure of the potassium channel: molecular basis of $K^+$ conduction and selectivity. *Science* **280**, 69–77 (1998).
4. Kuo, A. *et al.* Crystal structure of the potassium channel KirBac1.1 in the closed state. *Science* **300**, 1922–1926 (2003).
5. Zhou, Y., Morais-Cabral, J.H., Kaufman, A. & MacKinnon, R. Chemistry of ion coordination and hydration revealed by a $K^+$ channel–Fab complex at 2.0 A resolution. *Nature* **414**, 43–48 (2001).
6. Jiang, Y. *et al.* Crystal structure and mechanism of a calcium-gated potassium channel. *Nature* **417**, 515–522 (2002).
7. Long, S.B., Campbell, E.B. & Mackinnon, R. Crystal structure of a mammalian voltage-dependent Shaker family $K^+$ channel. *Science* **309**, 897–903 (2005).
8. Long, S.B., Tao, X., Campbell, E.B. & MacKinnon, R. Atomic structure of a voltage-dependent $K^+$ channel in a lipid membrane-like environment. *Nature* **450**, 376–382 (2007).
9. Cuello, L.G., Jogini, V., Cortes, D.M. & Perozo, E. Crystal structure of open-inactivated KcsA and the mechanism of C-type inactivation in $K^+$ channels. *Nature* **466**, 203–208 (2010).
10. Schoppa, N.E. & Sigworth, F.J. Activation of shaker potassium channels. I. Characterization of voltage-dependent transitions. *J. Gen. Physiol.* **111**, 271–294 (1998).
11. Cordero-Morales, J.F. *et al.* Molecular determinants of gating at the potassium-channel selectivity filter. *Nat. Struct. Mol. Biol.* **13**, 311–318 (2006).
12. Chakrapani, S., Cordero-Morales, J.F. & Perozo, E. A quantitative description of KcsA gating II: single-channel currents. *J. Gen. Physiol.* **130**, 479–496 (2007).
13. Zagotta, W.N., Hoshi, T. & Aldrich, R.W. Shaker potassium channel gating. III: Evaluation of kinetic models for activation. *J. Gen. Physiol.* **103**, 321–362 (1994).
14. Schrempf, H. *et al.* A prokaryotic potassium ion channel with two predicted transmembrane segments from *Streptomyces lividans*. *EMBO J.* **14**, 5170–5178 (1995).
15. Cuello, L.G., Romero, J.G., Cortes, D.M. & Perozo, E. pH-dependent gating in the *Streptomyces lividans* $K^+$ channel. *Biochemistry* **37**, 3229–3236 (1998).
16. Chapman, M.L. & VanDongen, A.M. K channel subconductance levels result from heteromeric pore conformations. *J. Gen. Physiol.* **126**, 87–103 (2005).
17. Zheng, J. & Sigworth, F.J. Selectivity changes during activation of mutant Shaker potassium channels. *J. Gen. Physiol.* **110**, 101–117 (1997).
18. Blunck, R., Cordero-Morales, J.F., Cuello, L.G., Perozo, E. & Bezanilla, F. Detection of the opening of the bundle crossing in KcsA with fluorescence lifetime spectroscopy reveals the existence of two gates for ion conduction. *J. Gen. Physiol.* **128**, 569–581 (2006).
19. Chakrapani, S., Cordero-Morales, J.F. & Perozo, E. A quantitative description of KcsA gating I: macroscopic currents. *J. Gen. Physiol.* **130**, 465–478 (2007).
20. Pusch, M., Bertorello, L. & Conti, F. Gating and flickery block differentially affected by rubidium in homomeric KCNQ1 and heteromeric KCNQ1/KCNE1 potassium channels. *Biophys. J.* **78**, 211–226 (2000).
21. Demo, S.D. & Yellen, G. Ion effects on gating of the $Ca^{2+}$-activated $K^+$ channel correlate with occupancy of the pore. *Biophys. J.* **61**, 639–648 (1992).
22. LeMasurier, M., Heginbotham, L. & Miller, C. KcsA: it's a potassium channel. *J. Gen. Physiol.* **118**, 303–314 (2001).
23. Choe, H., Sackin, H. & Palmer, L.G. Gating properties of inward-rectifier potassium channels: effects of permeant ions. *J. Membr. Biol.* **184**, 81–89 (2001).
24. Lu, T., Wu, L., Xiao, J. & Yang, J. Permeant ion-dependent changes in gating of Kir2.1 inward rectifier potassium channels. *J. Gen. Physiol.* **118**, 509–522 (2001).
25. Lu, T. *et al.* Probing ion permeation and gating in a $K^+$ channel with backbone mutations in the selectivity filter. *Nat. Neurosci.* **4**, 239–246 (2001).
26. Zhou, M. & MacKinnon, R. A mutant KcsA $K^+$ channel with altered conduction properties and selectivity filter ion distribution. *J. Mol. Biol.* **338**, 839–846 (2004).
27. Haug, T., Olcese, R., Toro, L. & Stefani, E. Regulation of $K^+$ flow by a ring of negative charges in the outer pore of BKCa channels. Part II: Neutralization of aspartate 292 reduces long channel openings and gating current slow component. *J. Gen. Physiol.* **124**, 185–197 (2004).
28. Proks, P., Capener, C.E., Jones, P. & Ashcroft, F.M. Mutations within the P-loop of Kir6.2 modulate the intraburst kinetics of the ATP-sensitive potassium channel. *J. Gen. Physiol.* **118**, 341–353 (2001).
29. Morais-Cabral, J.H., Zhou, Y. & MacKinnon, R. Energetic optimization of ion conduction rate by the $K^+$ selectivity filter. *Nature* **414**, 37–42 (2001).
30. Dreyer, I., Michard, E., Lacombe, B. & Thibaud, J.B. A plant Shaker-like $K^+$ channel switches between two distinct gating modes resulting in either inward-rectifying or 'leak' current. *FEBS Lett.* **505**, 233–239 (2001).
31. Singer-Lahat, D., Dascal, N. & Lotan, I. Modal behavior of the $K_v1.1$ channel conferred by the $K_v\beta1.1$ subunit and its regulation by dephosphorylation of $K_v1.1$. *Pflugers Arch.* **439**, 18–26 (1999).
32. Cooper, E. & Shrier, A. Inactivation of A currents and A channels on rat nodose neurons in culture. *J. Gen. Physiol.* **94**, 881–910 (1989).
33. Armstrong, C.M. & Gilly, W.F. Fast and slow steps in the activation of sodium channels. *J. Gen. Physiol.* **74**, 691–711 (1979).
34. Howe, J.R. & Ritchie, J.M. Multiple kinetic components of sodium channel inactivation in rabbit Schwann cells. *J. Physiol. (Lond.)* **455**, 529–566 (1992).
35. Lenaeus, M.J., Vamvouka, M., Focia, P.J. & Gross, A. Structural basis of TEA blockade in a model potassium channel. *Nat. Struct. Mol. Biol.* **12**, 454–459 (2005).
36. Bockenhauer, D., Zilberberg, N. & Goldstein, S.A. KCNK2: reversible conversion of a hippocampal potassium leak into a voltage-dependent channel. *Nat. Neurosci.* **4**, 486–491 (2001).
37. Levin, G. *et al.* Phosphorylation of a $K^+$ channel alpha subunit modulates the inactivation conferred by a beta subunit. Involvement of cytoskeleton. *J. Biol. Chem.* **271**, 29321–29328 (1996).
38. Cordero-Morales, J.F. *et al.* Molecular driving forces determining potassium channel slow inactivation. *Nat. Struct. Mol. Biol.* **14**, 1062–1069 (2007).
39. Capener, C.E., Proks, P., Ashcroft, F.M. & Sansom, M.S. Filter flexibility in a mammalian K channel: models and simulations of Kir6.2 mutants. *Biophys. J.* **84**, 2345–2356 (2003).

40. Domene, C., Klein, M.L., Branduardi, D., Gervasio, F.L. & Parrinello, M. Conformational changes and gating at the selectivity filter of potassium channels. *J. Am. Chem. Soc.* **130**, 9474–9480 (2008).
41. Bernèche, S. & Roux, B. Molecular dynamics of the KcsA $K^+$ channel in a bilayer membrane. *Biophys. J.* **78**, 2900–2917 (2000).
42. Shrivastava, I.H. & Sansom, M.S. Simulations of ion permeation through a potassium channel: molecular dynamics of KcsA in a phospholipid bilayer. *Biophys. J.* **78**, 557–570 (2000).
43. Guidoni, L., Torre, V. & Carloni, P. Water and potassium dynamics inside the KcsA $K^+$ channel. *FEBS Lett.* **477**, 37–42 (2000).
44. Bernèche, S. & Roux, B. A gate in the selectivity filter of potassium channels. *Structure* **13**, 591–600 (2005).
45. Nishida, M., Cadene, M., Chait, B.T. & MacKinnon, R. Crystal structure of a Kir3.1-prokaryotic Kir channel chimera. *EMBO J.* **26**, 4005–4015 (2007).
46. Delcour, A.H., Lipscombe, D. & Tsien, R.W. Multiple modes of N-type calcium channel activity distinguished by differences in gating kinetics. *J. Neurosci.* **13**, 181–194 (1993).
47. Luvisetto, S. *et al.* Modal gating of human CaV2.1 (P/Q-type) calcium channels: I. The slow and the fast gating modes and their modulation by beta subunits. *J. Gen. Physiol.* **124**, 445–461 (2004).
48. Yue, D.T., Herzig, S. & Marban, E. Beta-adrenergic stimulation of calcium channels occurs by potentiation of high-activity gating modes. *Proc. Natl. Acad. Sci. USA* **87**, 753–757 (1990).
49. McManus, O.B. & Magleby, K.L. Kinetic states and modes of single large-conductance calcium-activated potassium channels in cultured rat skeletal muscle. *J. Physiol. (Lond.)* **402**, 79–120 (1988).
50. Rothberg, B.S., Bello, R.A., Song, L. & Magleby, K.L. High $Ca^{2+}$ concentrations induce a low activity mode and reveal $Ca^{2+}$-independent long shut intervals in BK channels from rat muscle. *J. Physiol. (Lond.)* **493**, 673–689 (1996).
51. Auerbach, A. & Lingle, C.J. Heterogeneous kinetic properties of acetylcholine receptor channels in *Xenopus* myocytes. *J. Physiol. (Lond.)* **378**, 119–140 (1986).
52. Milone, M. *et al.* Mode switching kinetics produced by a naturally occurring mutation in the cytoplasmic loop of the human acetylcholine receptor epsilon subunit. *Neuron* **20**, 575–588 (1998).
53. Naranjo, D. & Brehm, P. Modal shifts in acetylcholine receptor channel gating confer subunit-dependent desensitization. *Science* **260**, 1811–1814 (1993).
54. Popescu, G. & Auerbach, A. Modal gating of NMDA receptors and the shape of their synaptic response. *Nat. Neurosci.* **6**, 476–483 (2003).
55. Patlak, J.B., Gration, K.A. & Usherwood, P.N. Single glutamate-activated channels in locust muscle. *Nature* **278**, 643–645 (1979).
56. Huganir, R.L., Delcour, A.H., Greengard, P. & Hess, G.P. Phosphorylation of the nicotinic acetylcholine receptor regulates its rate of desensitization. *Nature* **321**, 774–776 (1986).
57. Levy, D.I. & Deutsch, C. Recovery from C-type inactivation is modulated by extracellular potassium. *Biophys. J.* **70**, 798–805 (1996).

## ONLINE METHODS

**Channel expression and purification.** WT and mutant KcsA, cloned in pQE32 vector, were expressed in *Escherichia coli* XL1-blue cells (Stratagene). Membrane preparations were made by homogenizing the cells and spinning them down at 100,000*g* for 1 h. Membrane pellets were then solubilized by incubating them with PBS buffer containing dodecylmaltoside at room temperature and then purified with a $Co^{2+}$-based metal-chelate chromatography resin (Talon resin, Clontech). The quality of the purified protein was checked by gel-exclusion chromatography using a Superdex-200 column (GE Healthcare).

**Electrophysiology and kinetic analysis.** Electrophysiological measurements were made by patch-clamp recordings in channel-reconstituted liposomes. Purified protein was reconstituted in asolectin vesicles by dilution with 200 mM KCl and 10 mM MOPS buffer at pH 7.0. Residual detergent was further removed by incubation with BioBeads (Bio-Rad). The channel-incorporated liposome suspension was then centrifuged for 2 h at 100,000*g* and the pellet was resuspended in 60 µl of KCl-MOPS buffer. A drop of the proteoliposome was placed on a glass slide and dried overnight in a desiccator at 4 °C. The sample was then rehydrated with 20 µl of buffer, which yielded giant liposomes. This preparation was suitable for patch-clamp recordings after ~2 h. For macroscopic currents, KcsA was reconstituted in a 1:100 (mass:mass) ratio of protein to lipid, whereas for single-channel studies we used a ratio of 1:10,000 (mass:mass). Currents were recorded under symmetrical conditions of 200 mM KCl and 10 mM MOPS buffer unless otherwise specified. Some of the critical experiments were also conducted in succinate buffer to ensure that the fundamental gating properties were not affected by MOPS (data not shown). Recording pipettes were pulled from thin-walled borosilicate glass and heat polished such that they had a bath resistance of 1–2 MΩ when filled with 200 mM KCl, 10 mM MOPS solution. All measurements in this study were conducted in the inside-out configuration of the patch-clamp technique. Experiments were carried out at room temperature (20–22 °C). Currents were elicited in response to pH jumps from 8.0 to 4.0 using an RCS-160 fast solution exchanger (Biologic), fed by gravity. During pH pulses, the membrane was held at +150 mV. Macroscopic currents were sampled at 5 kHz using an Axon 200-B patch-clamp amplifier. Single-channel currents were digitized at a sampling rate of 40 kHz and low-pass filtered to 5 kHz through an eight-pole Bessel filter.

**Kinetic analysis.** All kinetic analyses were done using the QuB suite of programs (http://www.qub.buffalo.edu). Drifts in baseline were adjusted using the baseline correction algorithms within the QuB preprocessing module. Current traces were idealized into noise-free open and close transitions using SKM, a segmental *k*-means algorithm (the Viterbi algorithm), based on a hidden-Markov-modeling procedure at full bandwidth[58]. The number of closed and open states that best described the data was identified by using a maximum likelihood criteria, after imposing a dead time of 25 µs.

**Crystallization of Glu71 mutants.** Glu71 mutants were expressed and purified as described above. E71I and E71Q were crystallized in the presence of an antibody Fab fragment by the sitting drop method, as described previously[38]. The crystals diffracted to Bragg spacings of 2.3 Å for E71I and 2.7 Å for E71Q. Data were collected on beamlines 22ID-D (SERCAT) and 23ID (GMCA) at the Advanced Photon Source and processed with HKL200067.

**Crystallographic analysis.** Structures were solved by molecular replacement, using only the Fab fragment and extracellular part of WT KcsA (PDB 1K4C) without the selectivity filter as a search model to reduce the biasing of model prediction, as the expected conformation was supposed to be different from the closed state. The selectivity filter was built with side chain density corresponding to Val76, Tyr78 and Asp80 as markers. Multiple cycles of refinement using CNS and manual rebuilding using the program O were carried out until the complete model was built into the electron density map and the *R*-factors were lowered. Data collection and refinement statistics are provided in **Table 2**.

**Molecular dynamics simulations.** The simulation system was represented by an atomic model of the various mutants of the closed KcsA channel, embedded in a membrane bilayer solvated by an aqueous solution of KCl. The model contained the KcsA tetramer, dipalmitoylphosphatidylcholine (DPPC) molecules, water molecules and $K^+$ ions in the cavity and at sites S1 and S3. More potassium and chloride ions were added to ensure electrical neutrality and mimic a 150 mM KCl concentration. The system was set up using the CHARMM program[59], following a previously described methodology[41]. Constant-pressure molecular dynamics simulations were carried out using the NAMD program[60]. Each mutant was simulated for 20 ns.


58. Qin, F., Auerbach, A. & Sachs, F. Estimating single-channel kinetic parameters from idealized patch-clamp data containing missed events. *Biophys. J.* **70**, 264–280 (1996).
59. Brooks, B.R. *et al.* CHARMM: A program for macromolecular energy, minimization and dynamics calculations. *J. Comput. Chem.* **4**, 187–217 (1983).
60. Phillips, J.C. *et al.* Scalable molecular dynamics with NAMD. *J. Comput. Chem.* **26**, 1781–1802 (2005).